Journal of Non-Crystalline Solids 616 (2023) 122461

Contents lists available at ScienceDirect

Journal of Non-Crystalline Solids

journal homepage: www.elsevier.com/locate/jnoncrysol

Short range order of glassy KSb_5S_8 by diffraction, EXAFS, vibrational spectroscopy and DFT calculations

P. Jóvári[a,*], A. Chrissanthopoulos[b,c], K.S. Andrikopoulos[b,d], I. Pethes[a], I. Kaban[e], S. Kohara[f], B. Beuneu[g], S.N. Yannopoulos[b,h]

[a] Wigner Research Centre for Physics, Institute for Solid State Physics, POB 49, Budapest H-1525, Hungary
[b] Foundation for Research and Technology Hellas – Institute of Chemical Engineering Sciences (FORTH/ICE-HT), P.O. Box 1414, Rio, Patras GR-26504, Greece
[c] Department of Chemistry, National and Kapodistrian University of Athens, Zografou 15784, Greece
[d] Department of Physics, University of Patras, Rio, Patras GR-26504, Greece
[e] IFW Dresden, Institute for Complex Materials, Helmholtzstr. 20, Dresden 01069, Germany
[f] Research Center for Advanced Measurement and Characterization, National Institute for Materials Science (NIMS), Ibaraki 305-0047, Japan
[g] Laboratoire Léon Brillouin, CEA-Saclay, Gif sur Yvette CEDEX 91191, France
[h] Department of Chemistry, University of Patras, Rio, Patras GR-26504, Greece

ARTICLE INFO

Keywords:
Glass structure
Diffraction
EXAFS
Reverse Monte Carlo simulation
Raman scattering

ABSTRACT

We report on a detailed experimental and simulation study of the short- and medium-range order of a potential phase change material – glassy KSb_5S_8. On the experimental side, diffraction techniques and EXAFS have been employed to record accurate structural data. Structural models have been generated by fitting multiple datasets simultaneously with the reverse Monte Carlo simulation technique. In addition, density functional theory was employed to study the structure and vibrational modes of selected clusters, representative of the glass structure. Unconstrained RMC simulation runs revealed that the average Sb-S coordination number is 3.18 ± 0.2, thus Sb is mostly threefold coordinated in the glassy state. The fraction of edge and corner sharing SbS_n polyhedra and distribution of bridging S atoms (Q^n distribution) have also been obtained. Distribution of bridging S atoms around Sb is similar in the crystalline and glassy states. DFT calculations assisted in the identification of a Raman mode at $\sim 468\ cm^{-1}$, assigned to hypervalent bonding (quasi-tetrahedral units) in the glass structure.

1. Introduction

The reversible crystal-glass transition and the accompanied changes in the electronic structure have provided support that glassy R_2S-Sb_2S_3 (R = K, Sr) alloys could be promising candidates for applications in optoelectronics and data storage [1,2]. These alloys also possess high nonlinear optical (NLO) response and a large contrast between the NLO response of the crystalline and amorphous phases, which are essential for phase change materials used in optical data storage. A profound understanding of the short- and medium-range structural order is crucial to relate the composition and physical properties of these glasses. The experimental determination of the short- and medium-range structural order of ternary glasses requires the combination of various techniques such as neutron and X-ray diffraction, EXAFS, Raman spectroscopy or NMR. While Ge-Sb-Te (GST) phase change materials have been extensively studied over the last two decades, much less attention has been paid for the non-crystalline phase of materials that belong to the R_2S-Sb_2S_3 family.

The present study attempts to clarify the structure of glassy KSb_5S_8 ($K_2S - 5Sb_2S_3$) by neutron and high energy X-ray diffraction, Sb K-edge EXAFS measurements and Raman spectroscopy. To facilitate assignment of the vibrational modes, the Raman spectrum of glassy KSb_5S_8 is compared with that of vitreous Sb_2S_3. Structural changes accompanied with the addition of K_2S are interpreted by means of density functional theory (DFT) calculations of various clusters with different sizes. Diffraction and EXAFS datasets are fitted simultaneously in the framework of reverse Monte Carlo (RMC) simulations [3,4]. Selected parameters of the short-range order (bond distances and coordination numbers) as well as the fraction of corner and edge sharing pyramids are determined and compared with those of crystalline KSb_5S_8. The comparison reveals that the environment of Sb atoms exhibits a great variability in different chemical environments due to hypervalent bonding

---

* Corresponding author.
E-mail address: jovari.pal@wigner.hu (P. Jóvári).

https://doi.org/10.1016/j.jnoncrysol.2023.122461
Received 17 March 2023; Received in revised form 5 June 2023; Accepted 13 June 2023

configurations that Sb atoms can accommodate. DFT calculations show that over-coordinated Sb units in the form of quasi-tetrahedral clusters may form in KSb_5S_8, while they are absent from the neat Sb_2S_3 glass.

2. Methods

2.1. Sample preparation

The glasses were prepared by mixing proper amounts of the elements (S: 99.9999% purity; Sb: 99.9999% purity and K: >99% purity) from Alfa Aesar. The procedure took place in an Ar gas filled glove box to avoid oxidation of the metals. The elements were placed in carefully cleaned (with HF solution) silica tubes, were degassed in a vacuum line and were flame sealed. To avoid sulfur evaporation that could change the nominal composition, silica ampoules of very low diameter 6 mm outer diameter – 4 mm inner diameter were used. After the first melting of the elements and their volume reduction due to mixing, the free volume of the ampoule was further reduced using a flame torch on the upper part of the ampoule. The sealed tubes were placed in a cylindrical oven whose temperature was gradually increased to 750 °C and were kept at this temperature for 24 h. Glasses were prepared by fast quenching to water and were subsequently annealed at ~200 °C for 1 h.

2.2. Measurements

The x-ray diffraction experiment ('XRD 1′) at room temperature was carried out at the high-energy x-ray diffraction beamline BL04B2 [5] at Spring-8 using a two-axis diffractometer dedicated for glass, liquid, and amorphous materials [6]. The energy of incident x-rays was 61.6 keV. The beam size of x-rays was 0.7 mm width and 2.5 mm height. The diffraction patterns of powder sample in a thin walled (10 μm) silica glass tube of 0.5 mm diameter (supplier: GLAS Müller Berlin) and an empty tube were measured in transmission geometry. The intensity of incident x-rays and scattered x-rays were detected by an ionization chamber filled with Ar gas and a Ge solid state detector, respectively. The collected data were corrected using standard programs. Absorption coefficients [7], incoherent scattering functions [8] and atomic scattering factors [9] were used for the corrections and normalization. The fully corrected data were normalized to Faber-Ziman [10] total structure factor $S(Q)$.

An additional high energy x-ray diffraction measurement ('XRD 2′) was carried out at the BW5 high energy station [11] at Hasylab, DESY Hamburg. The energy of the radiation was 100 keV. Raw data were corrected for deadtime, background scattering and changes in detector solid angle [12].

The neutron diffraction structure factor was measured at the 7C2 liquid and amorphous diffractometer at (LLB, CEA, Saclay). Powdered sample was filled into a thin walled vanadium can (5 mm diameter, 0.1 mm wall thickness). Raw intensities were corrected for detector efficiency, background scattering, absorption and multiple scattering [14, 13]. Neutron scattering lengths, absorption and incoherent scattering cross sections were taken from Ref. [15].

Sb K-edge extended X-ray absorption fine structure was measured at beamline C of Hasylab, DESY Hamburg. Finely ground powder of KSb_5S_8 was mixed with cellulose and pressed into a tablet. The transmission of the tablet was about 1/e around the absorption edge. Intensities were recorded by ionization chambers filled with Ar/N_2 mixtures. The Viper program [16] was used to obtain $\chi(k)$ EXAFS curves from raw data. k^3-weighted $\chi(k)$ curves were first Fourier-transformed to real space (k-range: 2–15 Å^{-1}). The r-space data was then back-transformed to k-space using a rectangular window over 1.44 - 2.57 Å (see Fig. 1). The resulting filtered $k^3\chi(k)$ curve was used as input in reverse Monte Carlo

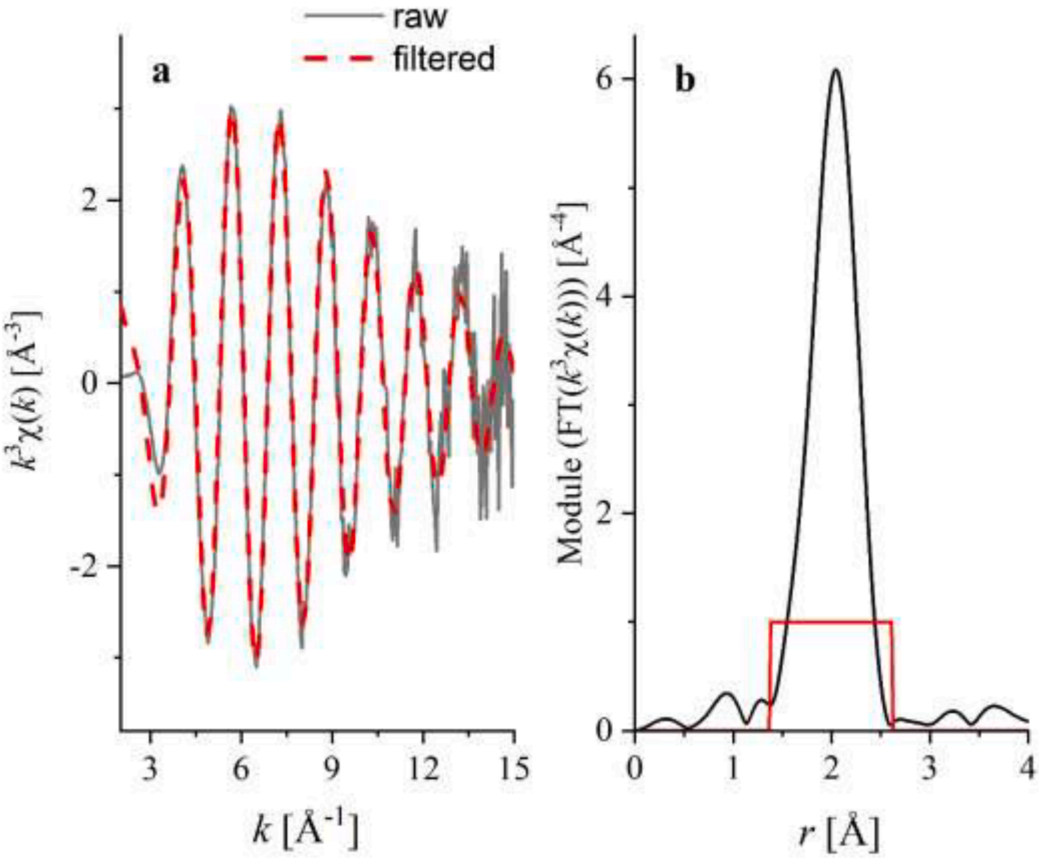

Fig. 1. (a) Raw and filtered k^3-weighted Sb K-edge EXAFS $\chi(k)$ curves of glassy KSb_5S_8 (b) Module of the Fourier transform of $k^3\chi(k)$. The red rectangle indicates the region used for back transformation.

simulation.

Raman spectra were recorded with the aid of a Fourier Transform Raman spectrometer (FRA 106/S, Bruker) operating at 1064 nm, using the backscattering geometry and a resolution of ~2 cm^{-1}. The laser energy (1.17 eV) is far from the absorption of the studied glasses, hence avoiding heat-induced or photo-induced effects.

2.3. Reverse Monte Carlo simulation

The reverse Monte Carlo simulation technique (RMC) is a general framework for modeling the structure of disordered materials by using experimental information (diffraction and/or EXAFS data) and physical constraints (density, minimum interatomic distances, coordination and bond angle constraints) as input information. RMC has been successfully applied several times to multicomponent covalent glasses [17,18]. For details of the simulation technique we refer to a paper describing rmcpp, the latest RMC version [4]. Backscattering coefficients needed to calculate model EXAFS spectra from the atomic configuration were obtained by the feff8.4 code [19].

The four datasets were fitted simultaneously. Minimum atomic distances (cut offs) were determined by a series of test runs in which the cut offs were increased gradually until fit qualities got worse or one or more peak shapes become distorted. This procedure gave well defined values in most cases. Due to the very low weight of K-K correlations fit qualities were not sensitive to the corresponding cut off. Finally, 4 Å was chosen. This value is arbitrary but within very broad limits (3 Å - 5 Å) the K-K cut off does not have any effect on the conclusions of this study. The values used to model the structure of KSb_5S_8 are summarized in Table 1. The density of glassy Sb_2S_3 is ~9% lower than that of its crystalline counterpart (4.21 $\mathrm{g/cm^3}$ vs. 4.62 $\mathrm{g/cm^3}$ – see Refs. [20,21]). It was assumed that the relative density difference of amorphous and crystalline KSb_5S_8 is the same. According to Berlepsch et al. the density of crystalline KSb_5S_8 is 4.18 $\mathrm{g/cm^3}$ [22] thus the density of the glassy phase was estimated to be 3.81 $\mathrm{g/cm^3}$. The corresponding number density is 0.0355$\mathrm{Å^{-3}}$.

Final simulations were started from two configurations:

(i) unconstrained 1: random array of points in a cubic box, satisfying only the cut off constraints (36,960 atoms)

(ii) unconstrained 2: a crystalline configuration, obtained in two steps. First the unit cell of crystalline KSb_5S_8 ($a = 8.1305$ Å, $b = 19.4800$ Å, $c = 9.0508$ Å, $\alpha = 90^\circ$, $\beta = 91.955^\circ$, $\gamma = 90^\circ$ [22]) was repeated $12 \times 5 \times 11$ times to get a configuration of 36,960 atoms (half box lengths: 48.824398 Å, 48.753250 Å, 49.841003 Å). Then β was set to 90° and the half box lengths were rescaled to 50.676 Å to get the required number density.

(iii) constrained: using the starting configuration of unconstrained 1 but eliminating unphysically low (0, 1 and 2) Sb-S coordination numbers up to 2.9 Å. This constraint was satisfied by 97% of the atoms.

The contribution of a given dataset to the total cost function is determined by its σ value [4]. In the present study the initial values were 0.01 for the neutron diffraction dataset, 0.01 and 0.014 for the XRD 2 and XRD 1 structure factors and 0.21 for the k^3-weighted EXAFS dataset. These values were reduced in 3 steps to 0.0006, 0.0006, 0.00085 and 0.014, respectively. The fits of the four experimental datasets and the partial pair correlation functions obtained by the simulation are shown in Figs. 2 and 3, respectively. The first minima of K-S and Sb-S partial pair correlation functions were taken as the upper limits of the first coordination spheres. Coordination numbers and nearest neighbor distances are listed in Tables 2 and 3. Fit qualities and partial pair correlation functions were practically the same for all starting configurations. Only $g_{KK}(r)$ exhibits visible differences but this pair correlation function has a very low weight in diffraction datasets due to the low concentration of K.

Table 1
Minimum distances (cut offs) applied in the reverse Monte Carlo simulation runs.

Pair	K-K	K-Sb	K-S	Sb-Sb	Sb-S	S-S
Cut off [Å]	4.0	3.0	2.4	3.0	2.2	2.7

Only Sb-S distances were taken into account in the reverse Monte Carlo fit of Sb K-edge data. Sb-S pairs were taken into account up to 2.9 A separation. Test runs with low Sb-Sb cut off (2.7 A) revealed that Sb-Sb bonding does not improve the fit quality and the resulting Sb-Sb coordination number (0.04) was well below the sensitivity of our approach (~0.3). For details of fitting EXAFS spectra with the reverse Monte Carlo simulation technique we refer to [23].

2.4. DFT calculations

The B3LYP hybrid density functional approach [24], which combines density functional and Hartree-Fock methods and uses Becke's three-parameter exchange functional [25] with the Lee-Yang-Parr correlation function [26] and its long-range corrected version using the Coulomb-attenuating method (CAM-B3LYP) [27], were employed as implemented in the GAUSSIAN 09 program package [28]. These methods were selected for the calculation of the structural details and vibrational properties. The equilibrium geometries of structural models have been fully optimized at the CAM-B3LYP/*LANL2DZ* level of theory using the Berny algorithm as implemented in Gaussian09 program package. All optimized geometries are characterized as stationary points on the potential energy surface with vibrational frequency calculations. The used basis sets for the hydrogen, potassium, sulfur and antimony are the Los Alamos National Laboratory *LANL2DZ* [29]. The choice of the basis sets is based on its ability to offer an effective core potential (ECP), which reduces the number of electrons that are considered explicitly and speeds up the calculations. It employs a core including for potassium and sulfur 10 electrons ([Ne]) and for antimony 46 electrons ([Kr] + 4d). For a more accurate description of the nature of the chemical bond between metal and sulfur and for a better prediction of the vibrational energies, the addition of diffuse p- function(s) as well as of polarization d- function(s) is necessary. A set of polarization functions for the main group atoms has been determined by Gilbert and co-workers and these are denoted as *LANL2DZpd* [30]. All basis sets were obtained from the EMSL Basis Set Library and the Basis Set Exchange (BSE) software [31].

3. Results and discussion

3.1. Reverse Monte Carlo analysis

The structure of crystalline Sb_2S_3 (stibnite) has been investigated by X-ray single crystal diffraction [21]. It was found that the basic structural motifs of the stibnite are Sb_4S_6 units. Each Sb atom in the unit has 7 nearest S neighbors. The 4 Sb atoms are located in two pairs of inequivalent sites. Sb atoms at one of these sites interact strongly with 3 close S neighbors located at distances in the range 2.52–2.54 Å, and weakly with 4 distant S neighbors located between 3.11 Å and 3.64 Å. Sb atoms at the other site have five close (below 2.9 Å) and two distant S neighbors (at 3.37 Å). The Sb_4Sb_6 units are linked to infinite chains by the long inter-unit Sb-S bonds (3.373 Å and 3.167 Å). These chains are also connected by weak Sb-S bonds to form two dimensional layers.

The structure of crystalline KSb_5S_8 can also be described in terms of two-dimensional layers of SbS_n polyhedra [22]. Sb atoms have 3, 4 and 5 S nearest neighbors and the mean Sb-S distance increases with Sb-S coordination number (threefold coordinated Sb: 2.47–2.51 Å, fivefold coordinated Sb: 2.675 Å). Neighboring SbS_n polyhedra share one or two common S atoms (the vast majority of S atoms have 2 or 3 Sb neighbors). K atoms are intercalated between the two-dimensional layers. The K-S coordination number is 9 while the mean K-S distance is 3.406 Å.

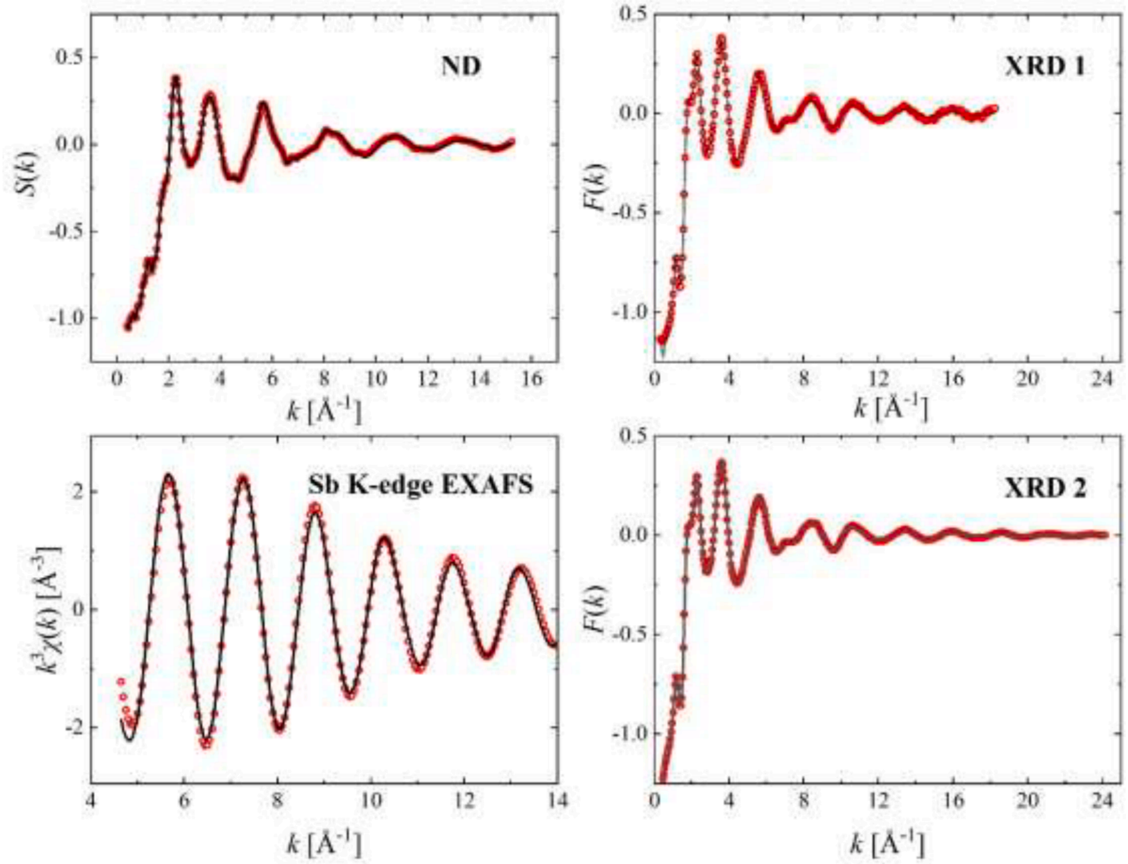

Fig. 2. Experimental diffraction and Sb K-edge EXAFS datasets and their fits obtained by reverse Monte Carlo simulation. XRD 1 and XRD 2 were measured at the photon energy of 61.6 keV and 100 keV, respectively (see the experimental section).

Our simulations show that in glassy KSb_5S_8, Sb atoms have on the average 3.18 ± 0.2 S neighbors located up to 2.9 Å and the mean Sb-S distance is 2.47 ± 0.02 Å. The small peaks at around 3.1 Å and ~3.6 Å coincide with some of the long Sb-S distances in crystalline Sb_2S_3 and KSb_5S_8 (see above). N_{SSb} is found to be 1.99 ± 0.15 indicating that the S atoms are mostly two-fold coordinated by 2 Sb neighbors. The mean K-S distance is about 3.4 Å in glassy KSb_5S_8 while the K-S coordination number is 7.69 ± 2.5.

Corner and edge sharing SbS_x polyhedra can be found in crystalline KSb_5S_8 (see Table 3.). Detailed investigation of the models of the glass revealed that about 58% of Sb-Sb pairs separated by a distance lower than 4.7 Å, have 1 common S neighbor while the fraction of edge-sharing SbS_n polyhedra (i.e. Sb-Sb pairs with two common S neighbors) is about 5–8%. Interestingly, the constraint model analysis yielded very similar values. About 34–35% of Sb-Sb pairs have no common S neighbor (topologically distant pairs).

Network connectivity can also be characterized by the Q^n distribution. In silicate and phosphate glasses Q^n gives the fraction of Si or P atoms connected to n bridging oxygens [32]. In the present case the fraction of bridging S atoms around Sb was investigated. Values for the crystalline starting configuration, unconstrained and constrained models are given in Table 4. The maximum of the Q^n distribution is in each case at $n = 3$ suggesting that the connectivity of SbS_x polyhedra is very similar in the crystalline and glassy states.

The structure of glassy Sb_2S_3 has been recently investigated by high energy X-ray diffraction, Raman scattering and density functional calculations [33]. It has been found that the Sb-S coordination number is 2.95 ± 0.04 and the mean Sb-S distance is 2.48 Å at room temperature. A small amount of Sb-Sb bonds was also observed (coordination number: 0.10 ± 0.05).

3.2. *Raman measurements*

Fig. 4(a) shows the FT-Raman spectra of glassy Sb_2S_3 and KSb_5S_8. The spectra reveal slight blueshift and broadening of the main band around 300 cm^{-1} for the KSb_5S_8 glass. In addition, the low energy band (~163 cm^{-1}) diminishes and a new band at high wavenumbers (~468 cm^{-1}) appears for this modified glass. To understand the structure of the KSb_5S_8 glass, we need first to identify the structural units present in glassy Sb_2S_3. Based on existing structural data, glassy Sb_2S_3 is mainly composed of $SbS_{3/2}$ pyramidal units linked by common corners. Early Raman spectra were recorded and analyzed by Watanabe et al. [34]. The authors observed two main bands at ~170 and ~290 cm^{-1}. Based on the Raman spectra of amorphous films of elemental Sb, which exhibit a strong band at ~150 cm^{-1}, it was concluded that the Raman spectra of the Sb_xS_{1-x} amorphous films show evidence for homonuclear Sb-Sb bonds forming $S_{2/2}Sb–SbS_{2/2}$ units. However, more detailed structural studies [20] provided strong support about the absence of Sb-Sb bonding in amorphous Sb_2S_3.

The C_{3v} symmetry of the pyramidal unit composing the structure of Sb_2S_3 glass yields the irreducible representation $\Gamma^{C}_{vib}3v = 2A_1$ (R,IR)+2E (R,IR), where all four modes are both Raman and IR active. The bands are typically denoted as ν_1 (symmetric stretching), ν_2 (symmetric bending), ν_3 (anti-symmetric/degenerate stretching) and ν_4 (degenerate bending). IR studies have suggested that ν_3 and ν_1 are located in the intervals 270–280 cm^{-1} and 300–310 cm^{-1}, respectively [35,36]. Using scaling arguments, based on the vibrational modes of $SbCl_3$, the ν_2 frequency of Sb_2S_3 is found to be at ~155 cm^{-1}, which is near the experimentally observed band at ~163 cm^{-1}.

KSb_5S_8 is the member of the $x\,(K_2S) \cdot y\,(Sb_2S_3)$ glass family with $x = 1$ and $y = 5$. Adding K_2S in the Sb_2S_3 network, offers additional S atoms beyond the stoichiometry of the Sb_2S_3. The presence of K atoms in the

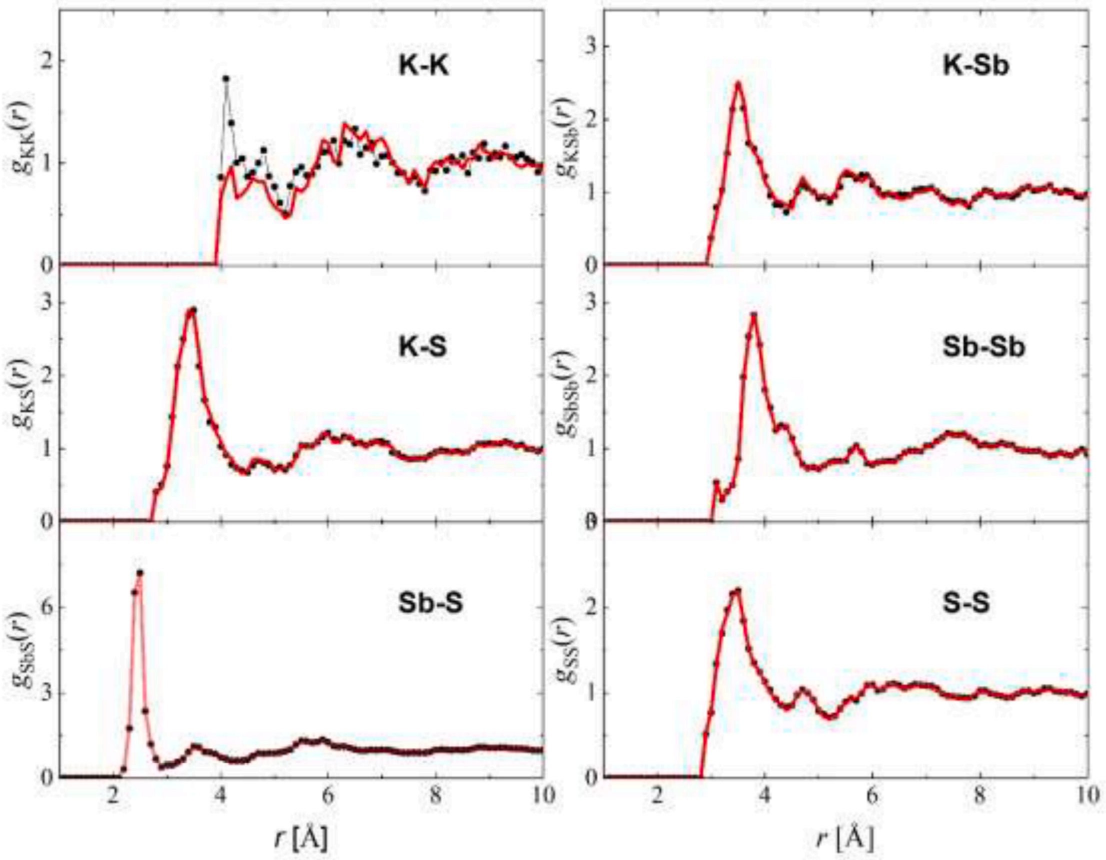

Fig. 3. Partial pair correlation functions of KSb_5S_8 obtained from random (line with symbols) and crystalline (red solid line) starting configurations.

Table 2
N_{ij} coordination numbers obtained by simultaneous modeling of the four experimental datasets. R_{ij}^{max} denotes the upper limit of the first coordination sphere.

Pair	K-S	S-K	Sb-S	S-Sb	K all	Sb all	S all
N_{ij}	7.68 ± 2.5	0.96 ± 0.3	3.18 ± 0.2	1.99 ± 0.15	7.68 ± 2.5	3.18 ± 0.2	2.95 ± 0.4
R_{ij}^{max}	4.4	4.4	2.9	2.9			

Table 3
Distribution of common S neighbors of pairs of Sb atoms obtained from the simulations using random and crystalline starting configurations. Values of the crystalline starting configuration are also given for comparison.

No. of common S neighbors	0	1	2
crystalline KSb_5S_8	0.429	0.500	0.071
unconstrained 1	0.334 ± 0.2	0.581 ± 0.2	0.085 ± 0.01
unconstrained 2	0.348 ± 0.2	0.578 ± 0.2	0.073 ± 0.01
constrained	0.354 ± 0.4	0.592 ± 0.5	0.053 ± 0.01

Table 4
Distribution of bridging S atoms around Sb in crystalline KSb_5S_8 as well as in the unconstrained and constrained models of glassy KSb_5S_8. The uncertainty is around 10% for Q^0 and Q^5 and 3% for the remaining Q values.

Q-species	Q^0	Q^1	Q^2	Q^3	Q^4	Q^5
crystalline KSb_5S_8	0	0	0.1	0.7	0.1	0.1
unconstrained 1	0.008	0.084	0.289	0.392	0.197	0.029
unconstrained 2	0.008	0.084	0.290	0.389	0.199	0.029
constrained	0.003	0.049	0.291	0.631	0.009	0.012

Sb_2S_3 glass is expected to interrupt the continuous character of the network, introducing negatively charged terminal Sb–S_t^- atoms, in analogy with alkali modifiers in oxide glasses. If such a mechanism prevails, the additional S atoms incorporated into the structure due to the K_2S content, compensate broken bridges forming additional Sb–S_t^- pairs. The K^+ ions should be located nearby the negatively charged terminal atoms, providing charge neutralization, see the schematic in Fig. 4(b). Sb–S_t^- bonds are shorter (stronger) than normal bridging Sb-S-Sb bonds. Pyramids that contain terminal bonds, $SbS_{2/2}S_t^-$, experience redistribution of the electronic density, which results to weakening of the other two bridging bonds of the same pyramidal units. First, fully-bridged, pyramid neighbors of such modified pyramids, will also be affected. Overall, strengthening of intramolecular vibrations of the pyramidal units takes place, which is evident by the blue shift of the main stretching vibrational frequencies in the Raman spectrum of the KSb_5Sb_8 glass.

Fig. 5 presents a deconvolution of the reduced Raman spectra of the Sb_2S_3 and the KSb_5S_8 glasses. The reduced representation of Raman spectra is essential for removing distortions in band intensities due to the thermal population factor and the Rayleigh scattering term. The Stokes–side reduced Raman intensity (I^{red}) is related to the experimentally measured one (I^{exp}) with the equation [37]:

$$I^{red}(\tilde{\nu}) = (\tilde{\nu}_0 - \tilde{\nu})^{-4}\tilde{\nu}\,[n(\tilde{\nu},T)+1]^{-1} I^{exp}(\tilde{\nu}), \quad (1)$$

where $n(\tilde{\nu},T) = [\exp(\hbar\tilde{\nu}/k_B T) - 1]^{-1}$ is the Bose-Einstein factor. The analysis of the reduced Raman spectra using Gaussian lines, resulted in the following main bands related to the intra-pyramidal vibrations: 273, 307 and 338 cm^{-1} for the Sb_2S_3 and 285, 322, and 352 cm^{-1} for the KSb_5S_8. The individual Gaussian lines are quite broad, as the number of fitting curves was kept the lowest possible. The first two correspond to the anti-symmetric stretching (ν_3) and symmetric stretching (ν_1) modes,

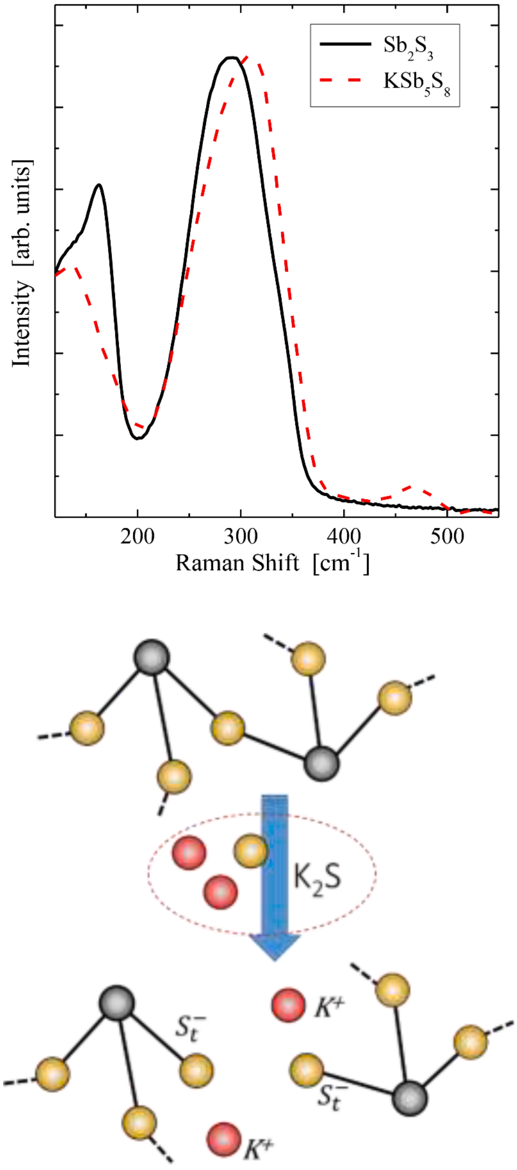

Fig. 4. (a) FT-Raman spectra of glassy Sb_2S_3 and KSb_5S_8. The spectra have been normalized to the maximum band intensity for better comparison. (b) Schematic illustration of the bridge breaking due to K_2S addition in Sb_2S_3.

respectively, according to the above discussion. The third peak represents vibrational modes of other species as will be described below. More insight into these modes will be presented below, based on the analysis of the theoretical Raman spectra emerging from DFT results.

A main issue to clarify is the presence of the band located at ~468 cm^{-1}. The wavenumber of this mode is reminiscent of S-S bonding in S-rich glasses or in glasses with S-rich domains due to nanoscale phase separation [38,39]. However, it is highly unexpected that such S-S bonding is present in the KSb_5S_8 glass structure for the reasons stated above. To understand the origin of the ~468 cm^{-1} band, DFT calculations were performed for a number of small clusters representing various possible bonding configurations at the short and medium-range structural order. Fig. 5 (*left column*) illustrates the four different clusters whose geometry was optimized by DFT and their harmonic frequencies were calculated. The same clusters modified by the addition of K_2S are shown in the right column of Fig. 5. The types of clusters that were selected, Fig. 5(a)-(d), represent structural units with progressively increasing size, which allows us to evaluate the influence of the cluster size on the calculated properties.

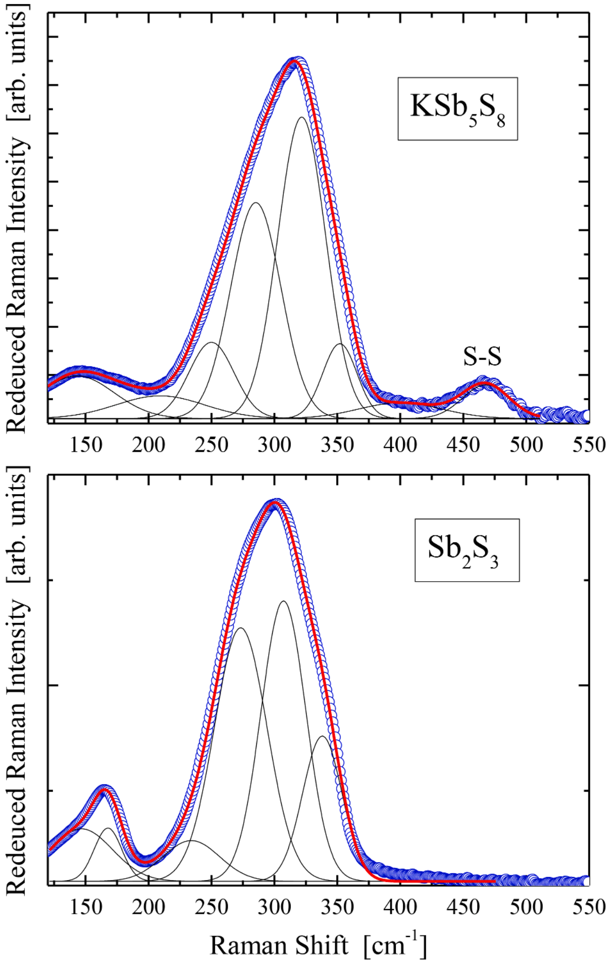

Fig. 5. Reduced Raman spectra of Sb_2S_3 and KSb_5S_8 deconvoluted by a set of Gaussian peaks.

Cluster (a) represents a cage-like structure of the form Sb_4S_6, where the absence of terminating H atoms simplifies the calculations.

Cluster (b) exemplifies a branching network-like structure arrangement of a central $Sb_2S_{3/2}$ pyramid bonded via corner sharing with three other pyramids.

Cluster (c) is a larger unit, which contains a ring of six pyramids interconnected via corner sharing.

Cluster (d) represents an enlargement of cluster (c) where each of the six pyramids have been bonded to an additional pyramid at axial arrangement.

For each of these four cases, a “K_2S unit” has been added and the new optimized geometry has been calculated. The respective structures are shown in the right column of Fig. 6. It should be noted that the optimized geometry for each cluster shown in Fig. 6, represents one possible stable configuration out of the various ones that these clusters can accommodate.

The analysis of broad Raman bands which emerge in spectra of glasses cannot be explained straightforwardly or unequivocally in terms of the molecular-like clusters or network-like structures present in glass structure. Especially, in heavy atoms glasses, such as Sb-S glasses, the experimental Raman spectrum shrinks in a featureless band where no spectral structure can be inferred, as shown in Fig. 5. As discussed, the deconvolution attempted for the experimental spectrum is indicative, in view of the lack of fine structure. The calculated Raman spectra of the four neat clusters and their K_2S-modified counterparts are shown in Fig. 7. The spectra were constructed using the respective Raman activities and the harmonic frequencies broadened by Gaussian lines using 4

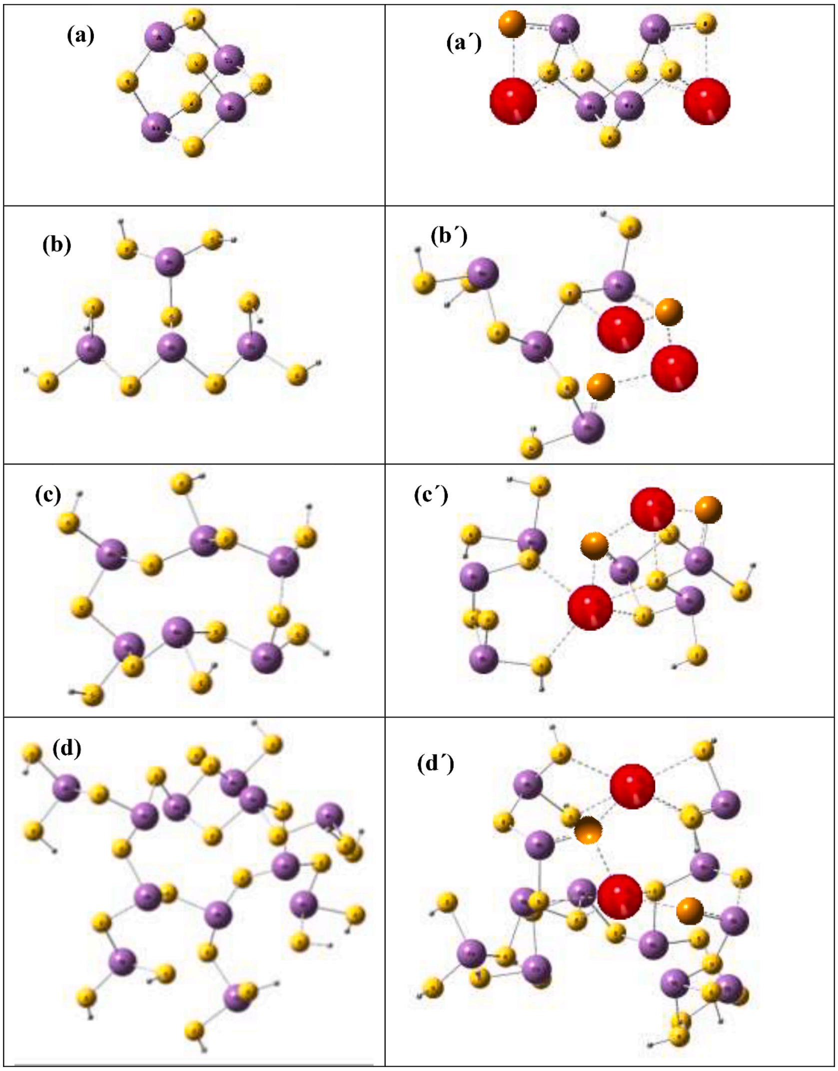

Fig. 6. (a)–(d): Optimized geometries of various structural models simulated by DFT. (a´) – (d´): The same structural models modified by addition of a K_2S molecule. See text for details. Color code: Sulfur (yellow spheres); Antimony (purple small spheres); Potassium (red spheres); Hydrogen (small gray spheres). Sulfur terminal atoms, S_t^- are marked by brown spheres.

cm^{-1} broadening. The spectra of the neat clusters are dominated by Sb-S vibrations with all S atoms being fully bridged (or H-terminated). The vibrations related to H atoms bending modes have been removed from the calculated spectra. The highest frequency of the vibrations is limited below 390 cm^{-1}. Three main zones define the origin of the vibrational modes, denoted in Fig. 7 as bending/deformation, stretching and terminal modes, although the distinction in the limits of the various zones may be not very sharp. The bands in the symmetric-stretching (SS) zone exhibit the lowest calculated depolarization ratio, which signifies their symmetric character, while the anti-symmetric stretching (aSS) modes are characterized by much higher values of the depolarization ratio. As the cluster size grows, from (a) to (d), the network-like character of the structure lowers the C_{3v} symmetry of the pyramidal unit and the respective vibrational modes attain a mixed character. The calculated Raman spectra of the K_2S-modified Sb_2S_3 glass demonstrate that the bands located at wavenumbers higher than ~400 cm^{-1} correspond to the terminal Sb–S_t^- bonds. Based on the theoretical description of the Raman bands situated in the spectral range 200–400 cm^{-1}, we can conclude that the individual bands deconvoluted in the experimental Raman spectrum, Fig. 5, are mainly symmetric and anti-symmetric stretching modes. The lowering of the C_{3v} symmetry creates a distribution of lower symmetry units, whose SS and aSS frequencies mix, and in certain cases more than one type of SS or aSS modes may appear.

The addition of K_2S engenders scission of Sb-S-Sb bridges between pyramidal units, leading to the formation of S_t atoms, as shown in the Fig. 6. For cluster (b´) the terminal frequencies are found slightly below 400 cm^{-1} due to the longer terminal bond length. The two terminal S_t^- atoms are not identical, thus resulting in separate frequencies at 377 and 391 cm^{-1}. Similar observations hold for cluster (c´) where the two inequivalent Sb–S_t^- bonds give rise to frequencies at ~372 and ~421 cm^{-1}. These observations reveal that the Sb–S_t^- bond strength, and consequently the vibrational frequency, depend strongly on the detailed configuration of K^+ ions around the terminal S_t^- atoms. Depending on the number of S atoms around K^+ ions and their mutual distance, DFT simulations have shown that the Sb–S_t^- terminal bond vibrates within the range 390 and 430 cm^{-1}. This finding demonstrates the strong sensitivity of the vibrational frequency on the local arrangement of K – S coordination sphere. The clusters simulated here represent small fragments of the true structure where only a few S atoms are found around K^+ ions. As the RMC analysis has shown, the average coordination between K and S is ~8 (see below). This means that under the presence of several S atoms around K^+, the influence of the latter, on the S_t^- atoms, decreases, which leads to strengthening of the Sb–S_t^- bonds. However, considering that DFT calculated harmonic frequencies are overestimated in relation to the experimental values by ~8–10% [40], the analysis presented above reveals that the existence of simple Sb–S_t^- terminal

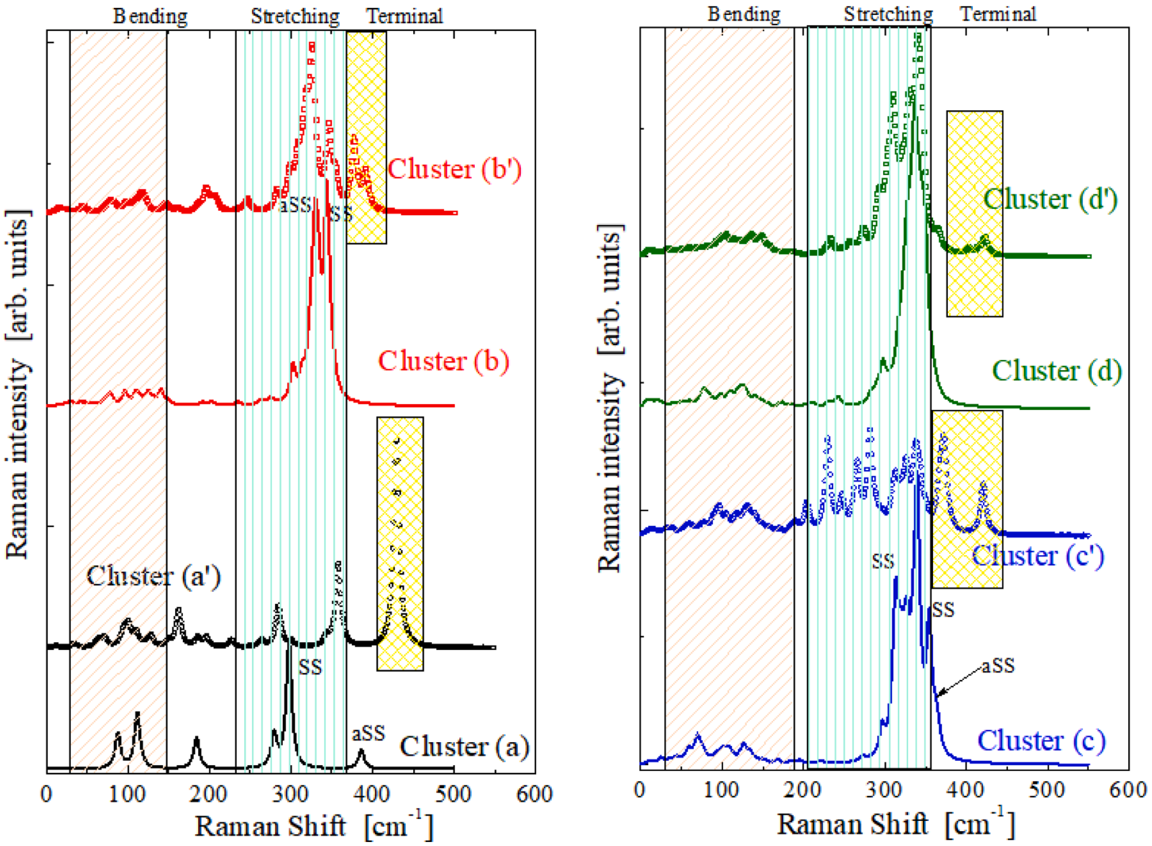

Fig. 7. Theoretical Raman spectra calculated from the harmonic frequencies determined by DFT for the clusters shown in Fig. 5, using line broadening of 4 cm^{-1}.

bonds does not suffice to account for the experimentally observed Raman band near 468 cm^{-1}. Indeed, the theoretical values scaled by correction factors will result in Sb–S_t^- vibrational modes in the range 360 and 400 cm^{-1}, which is still far below the experimental band at ~468 cm^{-1}.

The large difference between the DFT-calculated Sb–S_t^- mode energy and the experimental band calls for modification of the structural role of K_2S in the Sb_2S_3 glass. The average number of S atoms around Sb is 3.18 ± 0.2 meaning that the majority of Sb atoms are threefold coordinated but a degree of hypervalency is also tolerated by our models obtained by the simultaneous fit of three diffraction structure factors and an EXAFS dataset. Given that a ribbon-like structure is the main structural motif of the Sb_2S_3 crystal (stibnite), remnants of distorted ribbons could possibly be considered as the main structural motifs in the glass. Distortion, arising from disorder, can favor hypervalency in non-crystalline media [41]. Hypervalency is an interesting concept of chemical bonding introduced to account for the enhanced coordination that violates the electron-octet rule. Disorder may affect the Sb coordination sphere via the activation of the interactions with Sb 5s lone pairs. This will eventually influence the strength of the inter-ribbon interactions, rendering them stronger and assigning a more network-like character in the glass.

A possible hypervalent bonding configuration in non-crystalline chalcogenides is the so-called quasi-tetrahedral (QT) unit, sporadically invoked for As-based chalcogenides [42]. Fig. 8(a) illustrates the optimized geometries of three typical clusters which contain QT units. Cluster “1″ is a single QT unit; cluster “2″ represents an Sb_4S_6 unit which has the cage-like structure of β-P_4S_6 [43] which is called here β-Sb_4S_6; cluster “3″ is an Sb_6S_{10} unit which contains four interconnected QT species [44]. The corresponding Raman spectra are shown in Fig. 8(b), exhibiting strong bands near 465, 467, and 476 cm^{-1} for the clusters “1″, “2″, and “3″, respectively. This vibrational mode frequency is very near the experimentally observed band located at ~468 cm^{-1}. At the same time, the existence of QT units, in any form or configuration, provide also a rationale for the mean coordination number of Sb-S. Finally, it is important to note that beyond the clusters explored here, other configurations may also exist in the glass structure. However, the localized nature of the vibrational mode related to the terminal atom, imply its independence of the surrounding environment, testifying that the respective vibrational frequency will be within the range of wavenumbers mentioned above, i.e., 465–475 cm^{-1}.

4. Conclusions

In summary, we have attempted to provide a detailed analysis of the short and medium range structural order of glassy KSb_5S_8 using a number of experimental techniques and theoretical methods. In particular, the investigation included X-ray and neutron diffraction techniques, EXAFS and reverse Monte Carlo simulation, as well as DFT studies of clusters of various sizes. Various models of the glassy structure were analyzed and compared with crystalline KSb_5S_8. It was found that Sb atoms in the vitreous state are mostly threefold coordinated by S atoms with a significant contribution of higher coordination. The percentage of corner and edge sharing polyhedra and the distribution of bridging S atoms around Sb is similar in the crystalline and glassy states. DFT studies were used to explore a large number of clusters representative of neat Sb_2S_3 and KSb_5S_8, in an effort to illuminate the role of K_2S in the Sb_2S_3 glass and account for the spectral features observed in Raman spectra. The main finding is that the addition of K_2S does not cause the typical modification observed in oxide glasses upon alkali oxide addition. The presence of K_2S seems to favor hypervalent bonding exemplified by the signature of quasi-tetrahedral units in Raman spectra.

CRediT authorship contribution statement

P. Jóvári: Writing – review & editing, Formal analysis, Investigation,

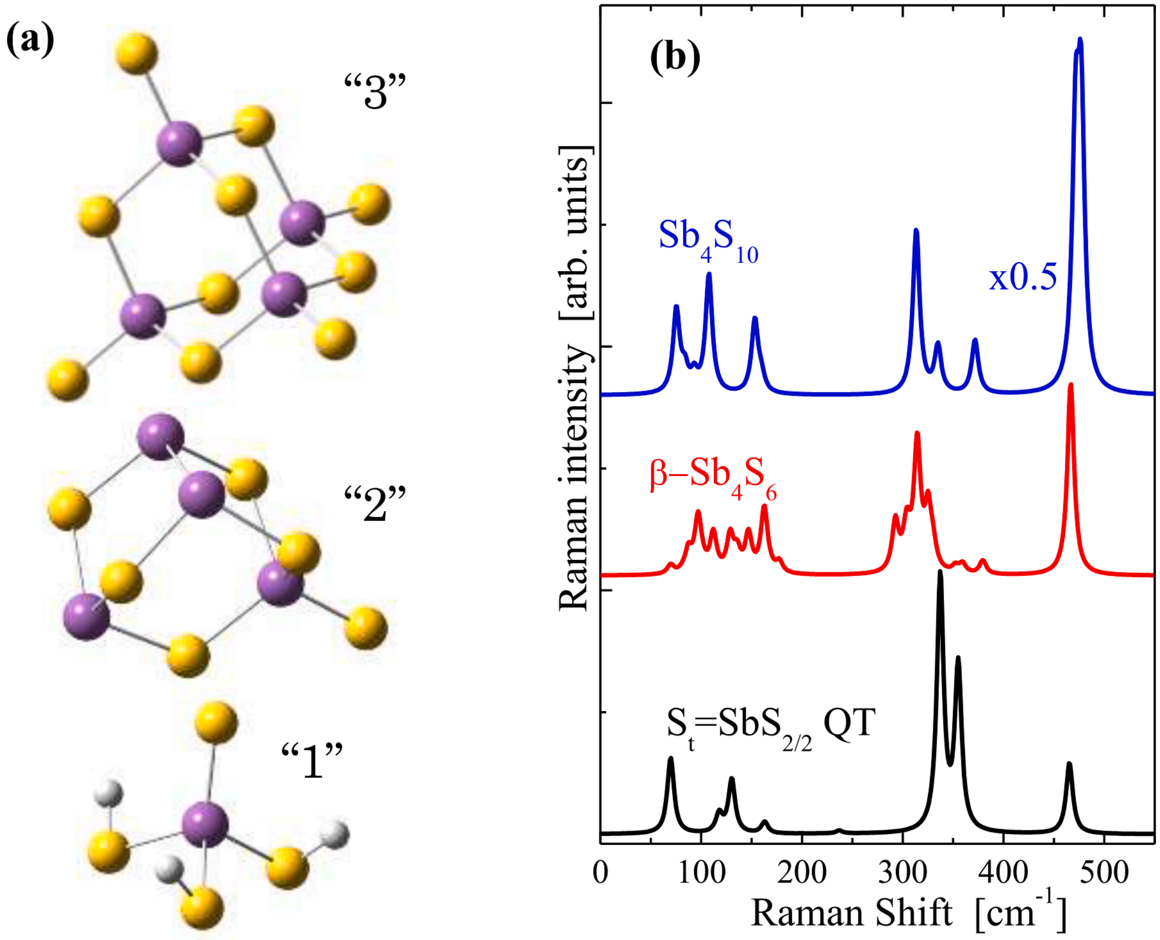

Fig. 8. (a) Optimized geometries of three typical clusters which contain QT units (see text for details). (b) Theoretical Raman spectra calculated from the harmonic frequencies determined by DFT for the clusters shown in (a), using line broadening of 4 cm^{-1}.

Data curation, Methodology, Funding acquisition. **A. Chrissanthopoulos:** Formal analysis, Investigation. **K.S. Andrikopoulos:** Formal analysis, Investigation. **I. Pethes:** Formal analysis, Investigation. **I. Kaban:** Data curation. **S. Kohara:** Data curation. **B. Beuneu:** Data curation. **S.N. Yannopoulos:** Writing – review & editing, Formal analysis, Investigation, Data curation, Methodology.

Declaration of Competing Interest

The authors declare that they have no known competing financial interests or personal relationships that could have appeared to influence the work reported in this paper.

Data availability

Data will be made available on request.

Acknowledgment

P.J. is indebted to L. Temleitner for helpful discussions. This work was supported by the ELKH project ‘Structure of materials used in energy storage’ (Grant No. SA-89/2021). The synchrotron radiation experiments were performed at BL04B2 of SPring-8 with the approval of the Japan Synchrotron Radiation Research Institute (JASRI) and at DORIS III (DESY, Hamburg), a member of the Helmholtz Association (HGF).

References

[1] W.F. Chen, B.W. Liu, S.M. Pei, Q.N. Yan, X.M. Jiang, G.C. Guo, ASb_5S_8 (A = K, Rb, and Cs): thermal switching of infrared nonlinear optical properties across the crystal/glass transformation, Chem. Mater. 33 (2021) 3729.
[2] T. Kyratsi, K. Chrissafis, J. Wachter, K.M. Paraskevopoulos, M.G. Kanatzidis, KSb_5S_8: a wide bandgap phase-change material for ultra high density rewritable information storage, Adv. Mater. 15 (2003) 1428.
[3] R.L. McGreevy, L. Pusztai, Reverse Monte Carlo simulation: a new technique for the determination of disordered structures, Mol. Simul. 1 (1988) 359.
[4] O. Gereben, P. Jóvári, L. Temleitner, L. Pusztai, A new version of the RMC++ Reverse Monte Carlo programme, aimed at investigating the structure of covalent glasses, J. Optoelectron. Adv. Mater. 9 (2007) 3021.
[5] M. Isshiki, Y. Ohishi, S. Goto, K. Takeshita, T. Ishikawa, High-energy X-ray diffraction beamline: BL04B2 at SPring-8, Nucl. Instrum. Methods A 467-468 (2001) 663.
[6] S. Kohara, M. Itou, K. Suzuya, Y. Inamura, Y. Sakurai, Y. Ohishi, M. Takata, Structural studies of disordered materials using high-energy x-ray diffraction from ambient to extreme conditions, J. Phys. Condens. Matter 19 (2007), 506101.
[7] S. Sasaki, X-ray absorption coefficients of the elements (Li to Bi, U) — KEK Report 90-16 (National Laboratory for High Energy Physics, Japan, 1991).
[8] J.H. Hubbell, Wm.J. Veigele, E.A. Briggs, R.T. Brown, D.T. Cromer, R.J. Howerton, Atomic form factors, incoherent scattering functions, and photon scattering cross sections, J. Phys. Chem. Ref. Data 4 (1975) 471–538.
[9] D. Waasmaier, A. Kirfel, New analytical scattering-factor functions for free atoms and ions, Acta Crystallogr. A 51 (1995) 416.
[10] T.E. Faber, J.M. Ziman:, A theory of the electrical properties of liquid metals III. The resistivity of binary alloys, Philos. Mag. 11 (1965) 153.
[11] R. Bouchard, D. Hupfeld, T. Lippmann, J. Neuefeind, H.-B. Neumann, H.F. Poulsen, U. Rütt, T. Schmidt, J.R. Schneider, J. Süssenbach, M. von Zimmermann, A triple-crystal diffractometer for high-energy synchrotron radiation at the HASYLAB high-field wiggler beamline BW5, J. Synchrotron Radiat. 5 (1998) 90.
[12] H.F. Poulsen, H.B. Neumann, J.R. Schneider, J. Neuefeind, M.D. Zeidler, Amorphous silica studied by high energy x-ray diffraction, J. Non Cryst. Solids 188 (1995) 63.

[13] I.A. Blech, B.L. Averbach, Multiple scattering of neutrons in vanadium and copper, Phys. Rev. 137 (1965) A1113.

[14] H.H. Paalman, J.C. Pings, Numerical evaluation of X14] absorption factors for cylindrical samples and annular sample cells, J. Appl. Phys. 33 (1962) 2635.

[15] V.F. Sears, Neutron scattering lengths and cross sections, Neutron News 3 (1992) 26.

[16] K.V. Klementev, Extraction of the fine structure from x-ray absorption spectraJ, Phys. D Appl. Phys. 34 (2001) 209.

[17] P. Jóvári, I. Kaban, J. Steiner, B. Beuneu, A. Schöps A. Webb, Local order in amorphous $Ge_2Sb_2Te_5$ and $GeSb_2Te_4$, Phys. Rev. B 77 (2008), 035202.

[18] H. Hashimoto, Y. Onodera, S. Tahara, S. Kohara, K. Yazawa, H. Segawa, M. Murakami, K. Ohara, Structure of alumina glass, Sci. Rep. 12 (2022) 516.

[19] A.L. Ankudinov, B. Ravel, J.J. Rehr, S.D. Conradson, Real-space multiple-scattering calculation and interpretation of x-ray-absorption near-edge structure, Phys. Rev. B 58 (1998) 7565.

[20] L. Červinka, A. Hruby, Structure of amorphous and glassy Sb_2S_3 and its connection with the structure of As_2X_3 arsenic chalcogenide glasses, J. Non Cryst. Solids 48 (1982) 231.

[21] P. Bayliss, W. Nowacki, Refinement of crystal structure stibnite, Sb_2S_3, Z. Kristallogr. 135 (1972) 308.

[22] P. Berlepsch, R. Miletich, Th. Armbruster, The crystal structures of synthetic KSb_5S_8 and $(Tl_{0.598}, K_{0.402})Sb_5S_8$ and their relation to parapierrotite ($TlSb_5S_8$), Z. Kristallogr. 214 (1999) 57.

[23] M. Winterer, Reverse Monte Carlo analysis of extended x-ray absorption fine structure spectra of monoclinic and amorphous zirconia, J. Appl. Phys. 88 (2000) 5635.

[24] A.D. Becke, Density-functional thermochemistry. III. The role of exact exchange, J. Chem. Phys. 98 (1993) 5648.

[25] P.J. Stephens, C.F. Devlin, M.J. Chabalowski, M.J. Frisch, Ab initio calculation of vibrational absorption and circular dichroism spectra using density functional force fields, J. Phys. Chem. 98 (1994) 11623.

[26] C. Lee, W. Yang, R.G. Parr, Development of the Colle-Salvetti correlation-energy formula into a functional of the electron density, Phys. Rev. B 37 (1988) 785.

[27] T. Yanai, D. Tew, N. Handy, A new hybrid exchange–correlation functional using the Coulomb-attenuating method (CAM-B3LYP), Chem. Phys. Lett. 393 (2004) 51.

[28] M.J. Frisch, G.W. Trucks, H.B. Schlegel, G.E. Scuseria, M.A. Robb, J.R. Cheeseman, G. Scalmani, V. Barone, B. Mennucci, G.A. Petersson, H. Nakatsuji, M. Caricato, X. Li, H.P. Hratchian, A.F. Izmaylov, J. Bloino, G. Zheng, J.L. Sonnenberg, M. Hada, M. Ehara, K. Toyota, R. Fukuda, J. Hasegawa, M. Ishida, T. Nakajima, Y. Honda, O. Kitao, H. Nakai, T. Vreven, J.A. Montgomery, Jr., J.E. Peralta, F. Ogliaro, M. Bearpark, J.J. Heyd, E. Brothers, K.N. Kudin, V.N. Staroverov, R. Kobayashi, J. Normand, K. Raghavachari, A. Rendell, J.C. Burant, S.S. Iyengar, J. Tomasi, M. Cossi, N. Rega, J.M. Millam, M. Klene, J.E. Knox, J.B. Cross, V. Bakken, C. Adamo, J. Jaramillo, R. Gomperts, R.E. Stratmann, O. Yazyev, A.J. Austin, R. Cammi, C. Pomelli, J.W. Ochterski, R.L. Martin, K. Morokuma, V.G. Zakrzewski, G.A. Voth, P. Salvador, J.J. Dannenberg, S. Dapprich, A.D. Daniels, O. Farkas, J.B. Foresman, J. V. Ortiz, J. Cioslowski, D.J. Fox, Gaussian 09, Revision A.01, Gaussian, Inc., Wallingford CT, 2009.

[29] (a) P.J. Hay, W.R. Wadt, Ab initio effective core potentials for molecular calculations. Potentials for K to Au including the outermost core orbital, J. Chem. Phys. 82 (1985) 299;
(b) W.R. Wadt, P.J. Hay, Ab initio effective core potentials for molecular calculations. Potentials for main group elements Na to Bi, J. Chem. Phys. 82 (1985) 284;
(c) P.J. Hay, W.R. Wadt, Ab initio effective core potentials for molecular calculations. Potentials for the transition metal atoms Sc to Hg, J. Chem. Phys. 82 (1985) 270.

[30] C.E. Check, T.O. Faust, J.M. Bailey, B.J. Wright, T.M. Gilbert, L.S. Sunderlin, Addition of polarization and diffuse functions to the LANL2DZ basis set for P-Block elements, J. Phys. Chem. A 105 (2001) 8111.

[31] B.P. Pritchard, D. Altarawy, B. Didier, T.D. Gibson, T.L. Windus, A New basis set exchange: an open, up-to-date resource for the molecular sciences community, J. Chem. Inf. Model. 59 (2019) 4814.

[32] U. Hoppe, A. Schöps, A.C. Hannon, A. Barz, D. Stachel, Structure of binary antimony phosphate glasses by diffraction methods, J. Non Cryst. Solids 583 (2022), 121476.

[33] M. Kassem, C.J. Benmore, A. Tverjanovich, T. Usuki, M. Khomenko, D. Fontanari, A. Sokolov, K. Ohara, M. Bokova, S. Kohara, E. Bychkov, Glassy and liquid Sb_2S_3: insight into the structure and dynamics of a promising functional material J, Mater. Chem. C 11 (2023) 4654.

[34] I. Watanabe, S. Noguchi, T. Shiizu, Study on local structure in amorphous Sb-S films by Raman scattering, J. Non Cryst. Solids 58 (1983) 35.

[35] M. Giehler, The effect of short-range order on the vibrational spectra of 3:2 coordinated chalcogenide glasses. analysis of the vibrational spectra by using pyramidal structural units, Phys. Status Solidi (b) 106 (1981) 193.

[36] M. Kato, S. Onari, T. Arai, Far infrared and Raman Spectra in $(As_2S_3)_{1-x}(Sb_2S_3)_x$ glasses, Jpn. J. Appl. Phys. 22 (1983) 1382.

[37] S.N. Yannopoulos, K.S. Andrikopoulos, Raman scattering study on structural and dynamical features of noncrystalline selenium, J. Chem. Phys. 121 (2004) 4747.

[38] F. Kyriazis, S.N. Yannopoulos, Colossal photostructural changes in chalcogenide glasses: athermal photoinduced polymerization in As_xS_{100-x} bulk glasses revealed by near-bandgap Raman scattering, Appl. Phys. Lett. 94 (2009), 101901.

[39] F. Kyriazis, A. Chrissanthopoulos, V. Dracopoulos, M. Krbal, T. Wagner, M. Frumar, S.N. Yannopoulos, Effect of silver doping on the structure and phase separation of sulfur-rich As–S glasses: raman and SEM studies, J. Non Cryst. Solids 355 (2009) 2010.

[40] M.L. Laury, M.J. Carlson, A.K. Wilson, Vibrational frequency scale factors for density functional theory and the polarization consistent basis sets, J. Comput. Chem. 33 (2012) 2380.

[41] T.H. Lee, S.R. Elliott, Hypervalency in amorphous chalcogenides, Nat. Commun. 13 (2022) 1458. Article number.

[42] P. Chen, C. Holbrook, P. Boolchand, D.G. Georgiev, K.A. Jackson, M. Micoulaut, Intermediate phase, network demixing, boson and floppy modes, and compositional trends in glass transition temperatures of binary As_xS_{1-x} system, Phys. Rev. B 78 (2008), 224208.

[43] R. Blachnik, U. Peukert, A. Czediwoda, B. Engelen, K. Boldt, Die Molekulare Zusammensetzung von erstarrten Phosphor-Schwefel-Schmelzen und die Kristallstruktur von β-P4S6, Z. Anorg. Allg. Chem. 621 (1995) 1637.

[44] E. Diemann, Rev. Chim. Miner. 16 (1979) 237.